J. Fluid Mech. (1991), *vol.* 231, *pp.* 325–343
Printed in Great Britain

Capillarity effects on surface gravity waves in a cylindrical container: wetting boundary conditions

By BRUNO COCCIARO, SANDRO FAETTI AND MAURIZIO NOBILI

Dipartimento di Fisica dell'Universita' di Pisa, Gruppo Nazionale di Struttura, della Materia del CNR, Istituto Nazionale di Fisica della Materia, Piazza Torricelli 2, 56100 Pisa, Italy

(Received 17 August 1990 and in revised form 25 March 1991)

Surface capillary–gravity waves are experimentally investigated in a cylindrical basin subjected to a horizontal oscillation by using a high-sensitivity optical method. We study the low-oscillation-amplitude regimes for a fluid which wets the vertical walls and we show that the presence of the capillary meniscus can effect greatly the main properties of the system. Both the free decay and the forced oscillations of surface oscillations are investigated. The amplitude, the phase and the damping of gravity waves are investigated in detail. The damping of the fundamental surface mode is found to exhibit nonlinear behaviour which is in qualitative agreement with the predictions of the Miles (1967) theory of capillary damping. The amplitude and the phase of gravity waves with respect to the oscillation of the container exhibit unusual behaviour which is strictly connected with the presence of the wetting boundary condition for the fluid at the vertical walls.

1. Introduction

The methods for calculating the frequencies and the damping coefficient of standing capillary–gravity waves in a closed basin are well known (see, for instance, Lamb 1932, chapter 9). Standard theoretical approaches assume that the free surface intersects the vertical walls orthogonally and the contact line at the three-phase interface (solid, liquid and air) can freely slip (*free-end edge boundary condition*). By making these assumptions the eigenfrequencies and the damping of the gravity waves in a cylindrical container can be obtained (Ursell 1952; Case & Parkinson 1957). According to Case & Parkinson (1957) the damping of capillary–gravity waves for a low-viscosity fluid is a function of the dimensionless small parameter

$$\epsilon = \left(\frac{2\nu k_n^2}{\omega_n}\right)^{\frac{1}{2}}, \tag{1.1}$$

where k_n is the wavenumber of the nth oscillation mode of the free surface, ν is the kinematic viscosity and ω_n is its angular eigenfrequency which is given, for an ideal fluid and free-end edge boundary conditions, by

$$\omega_n = \left[gk_n\left(1+\frac{T}{\rho g}k_n^2\right)\tanh(k_n h)\right]^{\frac{1}{2}}, \tag{1.2}$$

where g is the gravity acceleration, T is the surface tension, ρ is the mass density and h is the depth of the fluid. For low-viscosity fluids, as in the case of our experiment, ϵ is a very small parameter ($\epsilon \ll 1$) and thus, one can obtain the damping rate γ by using a perturbative procedure. Here γ is defined by $\eta_n(t) = \eta_n(0)\,e^{i\omega_n t}e^{\pi\gamma t}$ which

describes the free decay of surface oscillations of the nth mode. Many different mechanisms contribute to the damping of capillary–gravity waves in a cylindrical container of radius a:

(a) the viscous dissipation due to the motion in the bulk which gives the damping rate (Case & Parkinson 1957):

$$(\gamma_{\mathrm{b}})_n = \frac{\omega_n}{\pi}\epsilon^2; \tag{1.3}$$

(b) the viscous dissipation within the thin boundary layer near the walls of the container. At the first order in the small ϵ-parameter the corresponding damping rate is (Case & Parkinson 1957; Mei & Liu 1973):

$$(\gamma_{\mathrm{w}})_n = \frac{\omega_n \epsilon}{4\pi}\left[\frac{1}{k_n a}\frac{1+(n/k_n a)^2}{1-(n/k_n a)^2}+2\left(1-\frac{h}{a}\right)\mathrm{cosech}\,(2k_n h)\right], \tag{1.4}$$

where n is the number of the mode (for the complete definition of n see §2);

(c) other negligible contributions from the boundary dissipation at the free surface of the uncontaminated fluid (of the order of $(\nu)^{\frac{3}{2}}$ (see Ursell 1952).

By making a more sophisticated calculation Mei & Liu (1973) give also a correction of the angular frequency of the nth mode, due to the presence of a non-vanishing viscosity of the fluid, which is, at the first order in ϵ:

$$\omega_n = \left[gk_n\left(1+\frac{T}{\rho g}k_n^2\right)\tanh\,(k_n h)\right]^{\frac{1}{2}} - 2\pi(\gamma_{\mathrm{w}})_n. \tag{1.5}$$

All previous results have been obtained by assuming free-end edge boundary conditions at the vertical walls.

However, these ideal boundary conditions may not correspond to the real ones. In particular in most of the experiments, the contact angle θ between the fluid–air interface and the vertical walls can be different from 90° and thus a meniscus occurs near the walls. Furthermore some experiments (Dussan V. 1979) seem to indicate that the contact line may remain at rest also in the presence of a fluid motion (*pinned-end edge boundary condition*). In particular this new boundary condition seems to be appropriate to describe the edge constraint for a rim-full container. Benjamin & Scott (1979), Graham-Eagle (1983, 1984) and Douady (1988, 1990) use this new boundary condition for determining the eigenmodes and the eigenfrequencies of surface gravity waves in a rim-full container. The new boundary condition makes the theoretical analysis much more difficult.

In real systems we can expect that the behaviour of gravity waves could be somewhat more complex and intermediate between these two limiting cases (free-end edge and pinned-end edge boundary condition). In fact there is a large amount of experimental evidence (see, for instance, Dussan V. 1979) indicating that the behaviour of the contact line is very complex. According to the Young–Laplace equation the contact angle should be fixed and equal to θ_0 in static conditions. However, the experiments indicate that a range of possible static angles, centred on the Young–Laplace angle, is allowed to exist. This static range is exceeded when the contact line moves. For high enough speeds of the contact line the contact angles of advance and recession of the fluid assume two different and nearly constant values θ_{a} and θ_{r}. For small enough hydrodynamic velocities ($v < 0.4$ mm/s) the θ-angle varies continuously from the static values to the limiting dynamic values θ_{a} and θ_{r} as the velocity of the fluid increases. Therefore we can expect three main regimes as a function of the amplitude of gravity waves.

(i) A low-amplitude regime where the slope of the gravity wave at the vertical wall lies within the static range of contact angles. In this case the contact line can remain at rest and the hydrodynamic problem should be described by using the pinned-end edge boundary condition.

(ii) An intermediate-amplitude regime where the slope of the gravity wave exceeds the static range of contact angles and thus the contact line moves and the contact angle is an increasing function of the velocity.

(iii) A high-amplitude regime above a characteristic value of the velocity v_c where the contact angle of advancing and receding fluid have almost constant values (θ_a and θ_r) during the surface oscillation. We expect that this latter case could be described by the usual free-end edge boundary condition.

A very special case occurs when the contact angle between the fluid and the vertical walls is 0° (wetting boundary condition). In this case the contact line can move in only one direction, that of the liquid displacing the gas. In the opposite case (receding liquid), a thin layer of liquid is left behind.† The thickness of this layer depends upon the speed of the retreating liquid. This draining film could greatly influence the dynamic properties of the system and modify regimes (i), (ii) and (iii). Unfortunately, to the best of our knowledge no theoretical model concerning the effect of this film on the surface gravity waves has been proposed.

In two recent theoretical papers Hocking (1987*a*, *b*) proposed a new phenomenological linear boundary condition which partially simulates the complex behaviour of a real fluid–solid interface. To make the theoretical analysis possible he makes the simplifying assumptions that the static range of contact angles is negligibly small (regime (i) is absent) and the free surface of the fluid at rest is everywhere flat ($\theta_0 = 90°$). Furthermore he assumes that the contact angle increases linearly with the speed of the contact line. This model includes, as limiting cases, both the free-end and the pinned-end boundary conditions. By using this new boundary condition he calculates the eigenfrequencies and the damping rate of capillary–gravity waves in a rectangular uniform channel. The resulting theoretical expressions for the damping rate of surface waves and for the resonance frequency of the surface modes are very complex and their investigations require a numerical analysis. In the limiting cases (free-end and pinned-end) Hocking recovers the known results (Mei & Liu 1973; Case & Parkinson 1957).

The damping of capillary–gravity waves in the case of regimes (ii) and (iii) has been investigated theoretically by Miles (1967) who also assumes no static range of contact angles and a linear dependence of the contact angle on the velocity in the range (ii). Miles also considers the possible contribution of a thin viscoelastic film on the free surface. Therefore two new contributions to the damping rate are expected:

(*d*) the viscous dissipation at the free surface S characterized by the damping rate γ_s;

(*e*) the viscous dissipation due to capillary forces at the contact line L characterized by the damping rate γ_l.

The viscous dissipation rate at the free surface due to the presence of a surface viscoelastic film, at the first order in the small parameter ϵ, is found to be

$$(\gamma_s)_n = C_n \frac{\omega_n \epsilon}{2\pi} \coth(k_n h), \tag{1.6}$$

where the coefficient C_n is zero in the case of an uncontaminated free surface. If the free surface is covered by a thin viscoelastic film, C_n depends greatly on the

† This important point has been pointed out by one of the Referees.

properties of the surface film and on the number n of the mode. For the fundamental non-axisymmetric mode $n = 1$ of a cylindrical container of radius a, C_1 ranges from a minimum value $C_1 = 0$ to a maximum one $C_1 = 2$. $C_1 = 1$ for an inextensible surface film.

The size of the $(\gamma_1)_n$-capillary contribution to the damping rate has been estimated by Miles by assuming that the contact angle θ at the wall is a function of the hydrodynamic velocity v of the contact line according to the experimental evidence (e.g. Ablett 1923). Therefore a Coulomb-like frictional force

$$F = T(\cos\theta(v) - \cos\theta_0) \tag{1.7}$$

acts on the contact line between the fluid free surface and the walls. θ_0 is the static contact angle which is assumed to have a unique value (no regime (i)). An analytic expression for the damping rate $(\gamma_1)_n$ can be obtained by making the simplifying assumption that

$$\cos\theta(v) - \cos\theta_0 \approx \xi \frac{v}{v_c} \tag{1.8}$$

for $v \ll v_c$ (regime ii) and $\cos\theta(v) - \cos\theta_0 \approx \xi$ for $v \gg v_c$ (regime iii) where ξ is a dimensionless coefficient. For the fundamental mode $n = 1$ of a cylindrical container Miles (1967) obtains:

$$(\gamma_1)_1 = \gamma_1' = \frac{0.245\xi T k_1^2}{\rho v_c} \tanh(k_1 h) \tag{1.9}$$

for $v \ll v_c$, and

$$(\gamma_1)_1 = \gamma_1'' = \frac{0.398\xi T k_1^2}{\rho \omega_1 A} \tanh(k_1 h) \tag{1.10}$$

for $v > v_c$, where A is the maximum displacement of the free surface from its equilibrium position. In the case of water on wax, Ablett (1923) found $v_c \approx 0.4$ mm/s.

We notice here that the capillary damping rate of (1.10) exhibits a strong dependence on the A-displacement of the free surface. In the case of a cylindrical container of radius $a = 50$ mm, the resonance frequency is $\nu \approx 3$ Hz and, thus, the critical velocity v_c corresponds to a maximum displacement of the fluid at the vertical wall $A_c \approx v_c/2\pi\nu \approx 0.02$ mm, which is very small if compared with the radius a ($A_c/a \approx 0.0004$). Therefore the strongly nonlinear behaviour of (1.10) occurs when the oscillation amplitude of the free surface is still very much smaller than the typical amplitude values for which nonlinear gravitational effects can become relevant (Miles 1984).

Case & Parkinson (1957) measured the damping rate γ, for the first mode, for water in some cylindrical containers and compared their experimental results with the theoretical value of the viscous dissipation rate γ_w (equation (1.4)). They found that the ratio $\gamma/(\gamma_w)_1$ ranged from a maximum of 3 prior to polishing the cylindrical walls and approximated unity for a carefully polished brass cylinder. Therefore they infer that the observed discrepancies were related with the capillary effects at the walls $(\gamma_1)_1$. However, according to Miles, the presence of a surface inextensible layer on the free surface due to contamination (see Van Dorn 1966) could also explain the observed discrepancies. This mechanism seems to be the most relevant one in the case of the experiments performed by Keulegan (1959). Therefore a detailed investigation of the dependence of the damping rate on the free-surface maximum displacement A should contribute to clearly distinguish between these two different mechanisms since the contribution (1, 10) is strongly nonlinear.

Finally it should be remembered that the observed resonance frequencies of

surface waves often differ very much (e.g. Case & Parkinson 1957) from the theoretical one (equation (1.5)) calculated using the free-end edge boundary condition; in fact they can be greatly affected by the boundary conditions at the sidewalls of the container as showed by Benjamin & Scott (1979), Graham-Eagle (1983, 1984) and Douady (1988, 1990).

In this paper we report new experimental results concerning the low-amplitude regimes of surface capillary–gravity waves for a low-viscosity fluid (octane) in a cylindrical container. The resonance curves and the free decay of surface modes are investigated in detail by using a high-sensitivity optical apparatus which allows us to detect very low-amplitude surface oscillations. The case of a wetting boundary condition is investigated. Here 'wetting' means that the static contact angle is $\theta_0 = 0$. We find that the free decay of the fundamental surface mode ($k_1 a = 1.8412$) exhibits a non-exponential behaviour due to an amplitude dependence of the damping rate γ. The damping γ is found to decrease by increasing the amplitude of the surface oscillation. An analogous dependence on the amplitude is found for the eigenfrequency of the fundamental mode. This nonlinear behaviour is also found by looking at the resonance curve of the fundamental mode. The nonlinear dependence of the γ-coefficient is in qualitative agreement with the predictions of Miles' theory (equations (1.9) and (1.10)). However, we point out that Miles' theory does not account for the draining film which should be present for wetting boundary conditions. Therefore the qualitative agreement with our experimental results could be fortuitous. Finally the response of the free surface to a monochromatic horizontal oscillation of the container has been investigated in detail as a function of the excitation frequency (resonance curves for the gravity surface waves). The amplitude of the surface oscillations respectively in phase and 90° out of phase with the driving oscillation have been measured as a function of the oscillation angular frequency ω. In the case of wetting boundary conditions the eigenfrequencies of surface modes are satisfactorily described by (1.5), which can be deduced from the free-end edge boundary condition, but their amplitudes and phases exhibit an unusual behaviour which is not observed for different boundary conditions. The same qualitative features have been found by using water wetting a cylindrical container.

2. Surface capillary–gravity modes in a cylindrical container

In this section, for completeness, we remind readers briefly of the main theoretical results concerning the surface waves in a low-viscosity fluid contained in a cylindrical basin of radius a.

We consider a fluid of depth h subjected to a horizontal oscillation at the angular frequency ω. The local displacement $\eta(r, \theta, t)$ of the free surface with respect to the horizontal equilibrium position can be written as

$$\eta(r, \theta, t) = \eta_n(t)\, \psi_n(r, \theta), \tag{2.1}$$

where r and θ are planar polar coordinates (θ is the angle with respect to an horizontal x-axis), $\psi_n(r, \theta)$ are the eigenmodes of the surface, $\eta_n(t)$ are the amplitudes and the repeated indices are summed over the participating modes. The eigenmodes depend greatly on the kind of boundary conditions at the vertical walls. In the simplest case (free-end edge boundary conditions) the eigenmodes are given by

$$\psi_n \equiv \psi_{i,j}^{(c,s)} = N_{i,j}^{-1} J_i(k_{i,j} r)\,(\cos i\theta, \sin i\theta), \quad i = 0, 1, 2, \ldots, \quad j = 1, 2, 3, \ldots; \tag{2.2a}$$

$$J_i'(k_{i,j} a) = 0, \quad N_{i,j}^2 = \tfrac{1}{2}(1 + \delta_{0,i})\left\{1 - \left(\frac{i}{k_{i,j} a}\right)^2\right\} J_i^2(k_{i,j} a), \tag{2.2b, c}$$

where J_i is a Bessel function of the first kind and $k_{i,j}$ is one of the discrete set of eigenvalues given by the condition (2.2b). The superscripts c or s correspond, respectively, to the cosine or sine azimuthal dependence in (2.2a), respectively. For the fundamental non-axisymmetric mode ($n = 1; i = 1, j = 1$) the amplitude η_1 is related to the previously defined maximum displacement A (see (1.10)) by

$$A = \frac{\eta_1 J_1(k_{1,1} a)}{N_{1,1}}. \tag{2.2d}$$

If the basin is subjected to an oscillation $x(t) = x_0 \cos \omega t$ along the x-axis and nonlinear effects are negligible (Miles 1984), only the surface deformation showing the cosine θ-dependence with $i = 1$ can be excited. Therefore, in the following, we maintain the unique index n by setting $\psi_n \equiv \psi^{\mathrm{c}}_{1,n}$. The eigenfrequencies ω_n which correspond to the eigenmodes are given by (1.5) where $k_n \equiv k_{1,n}$. To the best of our knowledge, no exact theoretical expression for the equation of motion of the amplitude $\eta_n(t)$ of the nth mode in the presence of a forcing term has been proposed so far. Miles (1976, p. 424) made the simple assumption that the damping contribution to the generalized force is a linear function of the first time-derivative of the mode amplitude. Although this assumption seems to be reasonable, it is essentially a phenomenological assumption and its validity conditions are not well established. By making this assumption Miles found the following equation (here we neglect the nonlinear contribution):

$$F_n \cos \omega t = k_n^{-1} \coth k_n h (\ddot{\eta}_n + 2\pi\gamma_n \dot{\eta}_n + w_n^2 \eta_n), \tag{2.3}$$

where we have defined the amplitude of the generalized force

$$F_n = \omega^2 x_n x_0, \tag{2.4}$$

where x_0 is the oscillation amplitude of the basin ($x(t) = x_0 \cos \omega t$) and

$$x_n = (\pi a^2)^{-1} \int_0^a \int_0^{2\pi} x \psi_n \, r \, \mathrm{d}r \, \mathrm{d}\theta, \tag{2.5}$$

and where γ_n corresponds to the damping rate for the nth mode. For the fundamental mode ($n = 1$) one finds

$$k_1 = \frac{1.8412}{a}, \quad x_1 = 0.4968a, \quad N_{1,1} = 0.3455, \quad J_1(k_1 a) = 0.5819. \tag{2.6a–d}$$

Equation (2.3) can be easily solved to obtain the response of every mode to the excitation signal. For a fixed value of the generalized force F_n we find the standard Lorenzian resonance curve with a dephasing of 90° between $\eta_n(t)$ and the oscillation $x(t)$ of the vessel at the resonance frequency.

All these theoretical results hold only in the case of a free-end edge boundary condition. Much more complex results can be obtained by considering different boundary conditions such as the already cited pinned-end edge (Benjamin & Scott 1979; Graham-Eagle 1983, 1984) and the contact-angle boundary condition recently proposed by Hocking (1987a, b).

3. Experiment

3.1. *Apparatus*

The experimental set-up is the same as that used by Nobili *et al.* (1988) to investigate the nonlinear behaviour of surface gravity waves (see figure 1) and is similar to that used independently by Douady (1990).

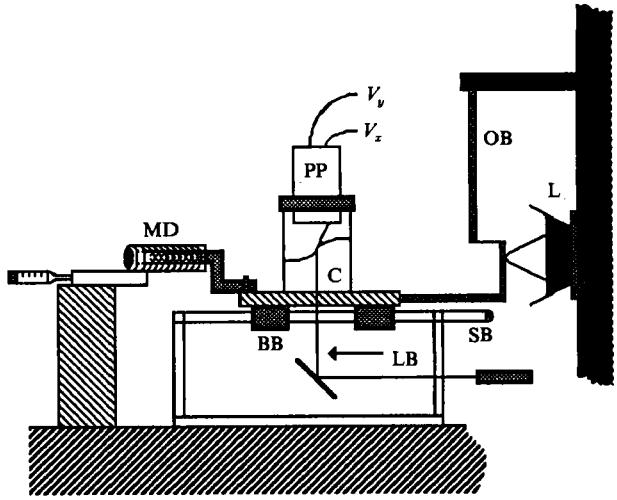

FIGURE 1. Schematic view of the experimental apparatus. L = loudspeaker; OB = brass bar; SB = stainless-steel bars; LB = laser beam; BB = ball-bearing; MD = electromagnetic device to measure the carriage displacement; C = cylindrical container; PP = position-sensitive photodetector.

The fluid (octane) is contained in a cylindrical tank of radius $a = 50.25$ mm. The container (C) is supported by a carriage with four ball-bearing (BB) that can slip on two horizontal stainless-steel bars (SB). The residual vibrations induced by this mechanical apparatus are negligible with respect to the smallest driving amplitude we use. The oscillation is driven by a 150 W loudspeaker (L) that is connected to the carriage and to the end of a brass bar (OB) stiffly connected at the other end to a vertical wall of the room. The brass bar ($8 \times 28 \times 126$ mm) allows the effects of the fluid recoil to be greatly reduced. Under these conditions we obtain, without any feedback loop, an amplitude stability of the carriage oscillation better than 0.1% and harmonic components less than 0.5%. The driving signal is produced by a synthesizer having a resolution of 1 mHz. The oscillation amplitude x_0 of the container is measured with a magnetic device (MD) having a minimum sensitivity of 1 μm and a linearity better than 0.5%. The local displacement $\eta(r, \theta, t)$ of the free surface is detected by means of a laser beam (LB) that impinges orthogonally on the bottom of the container, then is refracted by the free surface of the fluid and finally is collected by a dual-axis position-sensitive photodetector (PP). The photodetector gives two output signals (V_x and V_y) that are proportional to the displacement of the laser spot on the photosensitive surface of the photodetector with respect to its centre. Therefore these signals, for small enough η-values, are proportional to the spatial derivatives $\partial\eta/\partial x$ and $\partial\eta/\partial y$ at the incidence point (x_0, y_0), where x and y are the axes of the photodetector (x is oriented along the oscillation axis of the carriage). The laser beam is mounted on a two-axes precision translator which allows us to change in a continuous way the incidence point of the laser beam so that we can reconstruct the surface deformation η at each point of the free surface by integrating the output signals. The main advantages of this experimental apparatus are a very high sensitivity to surface deformations and the non-perturbative character of the method (no sensing element is introduced in the fluid). In particular, amplitudes of surface waves smaller than 1 μm can be easily detected. This allows us to investigate in detail the very low-amplitude regimes where the capillary effects can play an important role.

Two main kinds of experiments have been performed. In the first experiment the carriage oscillates at a frequency close to the resonance frequency of the fundamental mode and is stopped at a given time. The consequent decay of the output oscillating signal of the photodetector is recorded by using a digital waveform analyser (Data Precision-DATA6100). Three hundred and fifty free decay signals are averaged in such way as to reduce the spurious noise. Since the initial phase of the decay of surface oscillations is somewhat arbitrary, the average is performed by triggering the waveform analyser to correspond with the zero-crossing of the signal. An alternative and faster procedure to reduce the spurious noise consisted in constructing the auto-correlation function of the free decay signal.

In the second kind of experiment, the resonance curves of the surface eigenmodes were investigated by sweeping continuously the oscillation frequency of the loudspeaker and by measuring the response signals at the same frequency in phase and 90° out of phase with the oscillation $x(t)$ of the carriage. The sweep time was about two hours for each resonance curve. This time was chosen so that for each frequency point the acquisition time was much greater than the characteristic decay time ($\tau_n = 1/\pi\gamma_n < 100$ s). The experimental results were memorized on a computer and the characteristic parameters of each resonant mode (resonance frequency and half-width) were obtained by a numerical fitting procedure.

In order to confirm the generality of the observed phenomena we have also performed some partial measurements by using bi-distilled water. The wetting condition, in this case, was obtained by using a glass cylindrical container carefully washed with sulfochromic acid. The internal radii of the cylinders were 50.25 mm and 48.25 mm for octane and water respectively. In both cases the fluids wetted the vertical walls of the containers. The contact angle at the fluid–solid interface, for both fluids, was experimentally checked by measuring the refraction of a laser beam by the fluid wedge and was found to be zero within our experimental accuracy ($\Delta\theta_0 \leqslant 2°$).

3.2. *Free decay and resonance curve of the fundamental mode*

Before measuring the damping coefficient for the fundamental mode we measured the spatial shape of this mode. Figures 2(*a*) and 2(*b*) respectively show the experimental results concerning the dependences of $\partial\eta(r, \theta = 0)/\partial r$ and $\eta(r, \theta = 0)$ for octane. These two functions are indicated with the notations $\partial\eta/\partial x$ and $\eta(x)$ in figures 2(*a*) and 2(*b*), where x is the displacement from the centre of the free surface along the x-axis. The depth h of the fluid was 78 mm and the radius of the container was $a = 50.25$ mm. The solid lines in figure 2 correspond to the best fit of the experimental data using the function $\eta(x) = A(J_1(k_1 x)/J_1(k_1 a))$, with A as a free parameter. Within the accessible experimental range (up to ≈ 5 mm from the wall of the cylinder), the surface profile is in very good agreement with the predictions of the theory for a free-end edge boundary condition. Analogous results have been obtained using water. We remind readers that, for the fundamental mode, the maximum displacement A of the free surface is given by

$$A = \frac{2J_1(k_1 a)}{k_1} \frac{\partial\eta(r = 0, \theta = 0)}{\partial r} = 31.76 \frac{\partial\eta(r = 0, \theta = 0)}{\partial r} \text{mm}$$

(for $a = 50.25$ mm). Therefore, by measuring $\partial\eta(r = 0, \theta = 0)/\partial r$, we obtain the amplitude A.

The free decay of the surface fundamental mode in octane is shown in a linear and in a semi-logarithmic scale in figures 3(*a*) and 3(*b*) respectively. The vertical axes

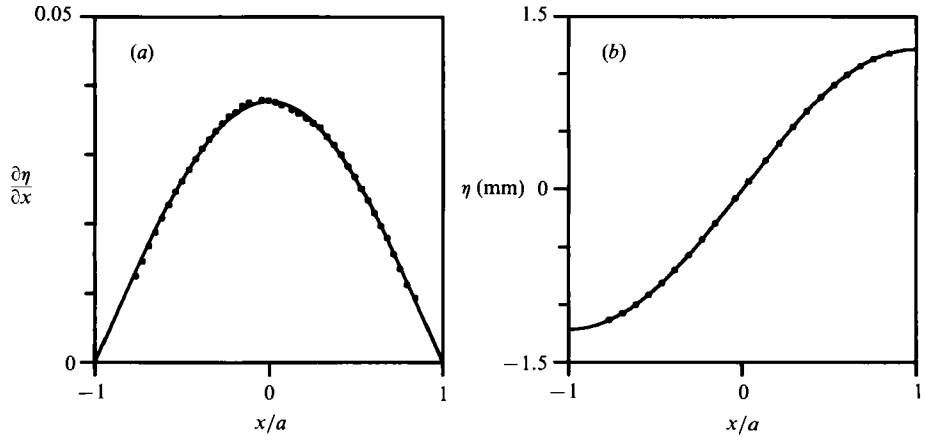

FIGURE 2. (*a*) Derivative $\partial\eta/\partial x$ of the surface displacement $\eta(x)$ versus the ratio between the distance x from the cylinder axis along the x-axis and the cylinder radius a. (*b*) Surface displacement $\eta(x)$ versus x/a as obtained by integration of the experimental points of (*a*). The oscillation amplitude of the carriage is $x_0 = 7.89 \times 10^{-3}$ mm; the depth of the fluid is $h = 78$ mm and the radius of the cylindrical container is $a = 50.25$ mm. The oscillation frequency ν corresponds to the resonance frequency for the fundamental mode ($\nu = 2.993$ Hz).

show the value of the amplitude A. A detail of the curve is shown in the insert of figure 3(*a*). The points in the insert are the experimental results whilst the solid line corresponds to the best fit made by using the local expression:

$$A(t) = A_T \, \mathrm{e}^{-\pi\gamma_T t'} \cos(2\pi\nu_T t' + \varphi_T), \tag{3.1}$$

where $t' = t - T$ and T is the value of time at the centre of the time interval $[t_1, t_2]$ (in the insert of figure 3(*a*), $t_1 = 24$ s, $t_2 = 28$ s and $T = \frac{1}{2}(t_1 + t_2) = 26$ s). A_T, γ_T, ν_T, φ_T are fit parameters that correspond to the oscillation amplitude, the damping rate, the frequency and the phase at the time T.

The slope of the curve in figure 3(*b*) increases with increasing time. This means that the damping coefficient must be a decreasing function of the oscillation amplitude of the fundamental mode. By using the previously defined fit procedure (see (3.1) and the insert in figure 3*a*), we have been able to obtain the dependence of γ and that of the oscillation frequency of the decay signal (it coincides practically with the resonance frequency ν_1 of the fundamental mode) on the amplitude A. The values for γ and ν_1 versus A are plotted in figures 4(*a*) and 4(*b*) respectively. The damping rate γ is almost constant and equal to $\gamma_0 \approx 34$ mHz for A lower than a characteristic value $A_c \approx 0.15$ mm, then it decreases to reach an almost constant value $\gamma_1 \approx 26$ mHz for $A \gg A_c$. The solid line in figure 4(*a*) corresponds to the best fit of the experimental results by using a trial function of the form:

$$\gamma = \gamma_0 + \frac{\Delta\gamma}{[1 + (A/A_c)^n]^{1/n}}, \tag{3.2}$$

where γ_0, $\Delta\gamma$ and A_c are fit parameters and n is chosen to be $n = 6$. This function has been chosen in such a way as to qualitatively reproduce the behaviour given by (1.9) and (1.10). In fact $\gamma \approx \gamma_0 + \Delta\gamma = \text{const.}$ for $A \ll A_c$ and $\gamma \approx \gamma_0 + \Delta\gamma A_c/A$ for $A \gg A_c$. By increasing the value of n one obtains a sharper transition from the $A < A_c$ regime to the other one. The quality of the fit remains almost the same for any value of n greater than 3.

The frequency ν_1 decreases continuously by increasing the amplitude A, from a

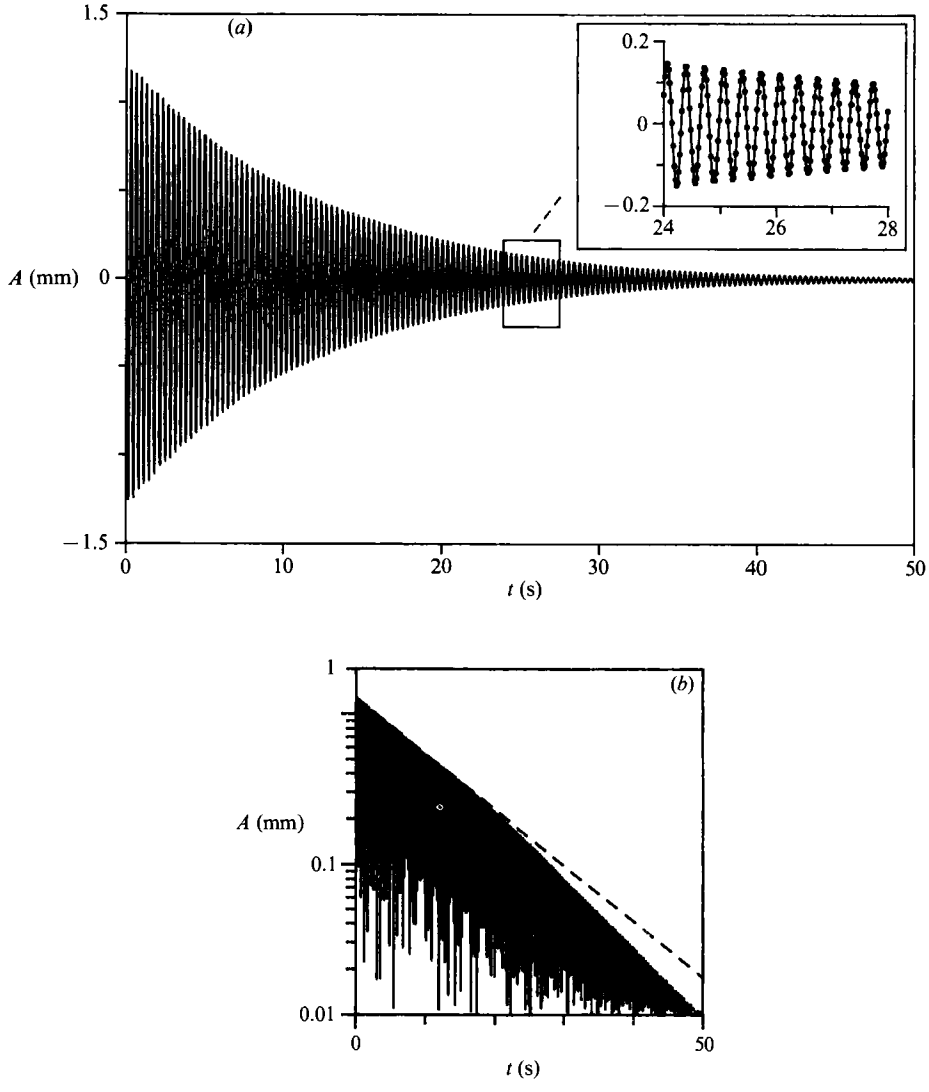

FIGURE 3. (*a*) Free decay of surface oscillation versus time. The vertical axis shows the value of the maximum displacement A at the cylinder ($A = \eta(a)$). In the insert a detail of the curve is shown. Points correspond to the experimental data whilst the solid line corresponds to the best fit to the theoretical form: $A(t) = A_T e^{-\pi\gamma_T t'} \cos(2\pi\nu_T t' + \varphi_T)$, where $t' = t - T$, with $T = 26$ s. (*b*) The free decay of (*a*) using a logarithmic scale on the vertical axis. The broken line shows the slope of the free decay at small times (larger amplitudes). The depth of the fluid is $h = 78$ mm and the radius of the cylindrical container is $a = 50.25$ mm.

maximum value of $\nu_1^0 \approx 2.997$ Hz, to a minimum value $\nu_2^1 \approx 2.990$ Hz. We note that the theoretical resonance frequency for the fundamental mode and for free-end edge boundary condition is given by (1.5). By using the known value of the surface tension T and of the kinematic viscosity ν of octane ($T = 21.80$ dynes/cm and $\nu = 0.00772$ cm^2 s^{-1}, Weast 1970) we obtain $\nu_1^{\text{th}} = 3.000$ Hz. If we compare this value with the limit value for $A \gg A_c$ we find $\nu_1^{\text{th}} - \nu_1^1 \approx 0.010$ Hz. Analogous dependences of γ and ν_1 on the amplitude A have been found by using water wetting a glass cylinder.

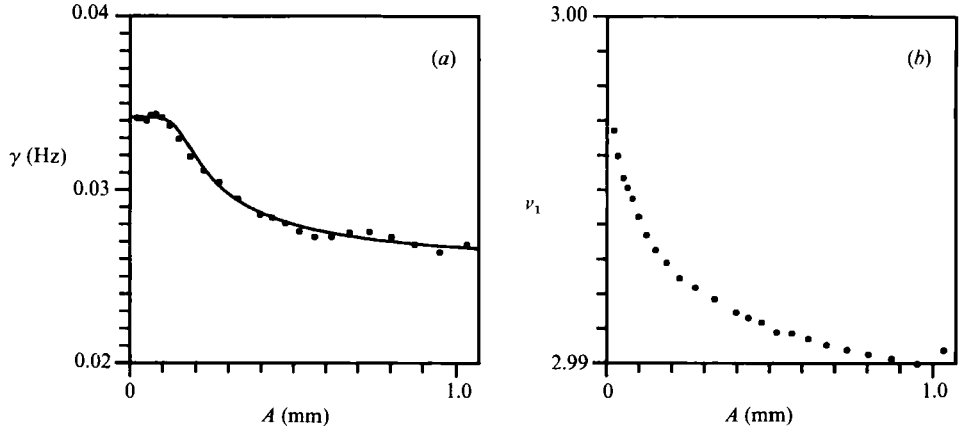

FIGURE 4. (*a*) Damping coefficient γ versus the maximum displacement A of the free surface for the fundamental mode. The solid line corresponds to the best fit of the experimental points using the trial function (3.2), where $n = 6$. The values of γ_0, $\Delta\gamma$ and A_c of the best fit are $\gamma_0 = 25.4$ mHz; $\Delta\gamma = 8.8$ mHz and $A_c = 0.145$ mm. (*b*) Frequency of the free damped oscillation of the surface versus the maximum displacement A. The depth of the fluid is $h = 78$ mm and the radius of the cylindrical container is $a = 50.25$ mm.

An alternative method to investigate the decay rate γ and the resonance frequency ν_1 of the fundamental mode consists of analysing the resonance curve. This curve is obtained by sweeping the oscillation frequency of the cylindrical tank at a constant amplitude of the generalized force F_n (see (2.4)). The experimental value of the maximum surface displacement A versus the frequency ν is shown in figure 5(*a*). The solid line corresponds to the best fit of the experimental results to the Lorenzian form:

$$A(\nu) = \frac{\bar{A}}{(\nu^2 - \nu_1^2)^2 + \gamma^2\nu^2}, \tag{3.3}$$

which can be obtained as a solution of (2.3) (with $n = 1$) by assuming no amplitude dependence for γ and ν_1. Far from the resonance frequency there is a small but significant difference between theory and experiment. One can easily show that this discrepancy is not due to the presence of higher-order surface modes since the contribution of these modes in this frequency range is completely negligible. Figure 5(*b*) shows the same experimental points as figure 5(*a*), whilst the solid line corresponds to the best fit obtained by using (3.3) with amplitude-dependent values of γ and ν_1 as in figures 4(*a*) and 4(*b*). We can see that within our experimental uncertainty ($\approx 2\%$) the solid line in figure 5(*b*) fits the experimental data well. Therefore both the damping curve and the resonance curve give strong evidence for nonlinear behaviour of the system at very small amplitudes. We note that the characteristic critical amplitude A_c where the nonlinear behaviour becomes evident (see figure 4*a*) is very small ($A_c \approx 0.15$ mm) and corresponds to a critical hydrodynamic velocity on the sidewall $v_c = \omega A \approx 2.83$ mm/s. These amplitudes are much smaller than those for which the effects due to nonlinear coupling between modes play some role (Miles 1984; Funakoshi & Inoue 1988; Nobili *et al.* 1988).

To the best of our knowledge so far the only theoretical model which can account for an amplitude dependence of the decay rate qualitatively similar to that shown in figure 4(*a*) is the Miles theory of capillary damping. In particular, as experimentally observed, this model predicts that the damping coefficient γ assumes its maximum and constant value for very low amplitudes ($v < v_c$) ($\gamma = (\gamma_w)_1 + (\gamma_b)_1 + (\gamma_s)_1 + \gamma_1'$),

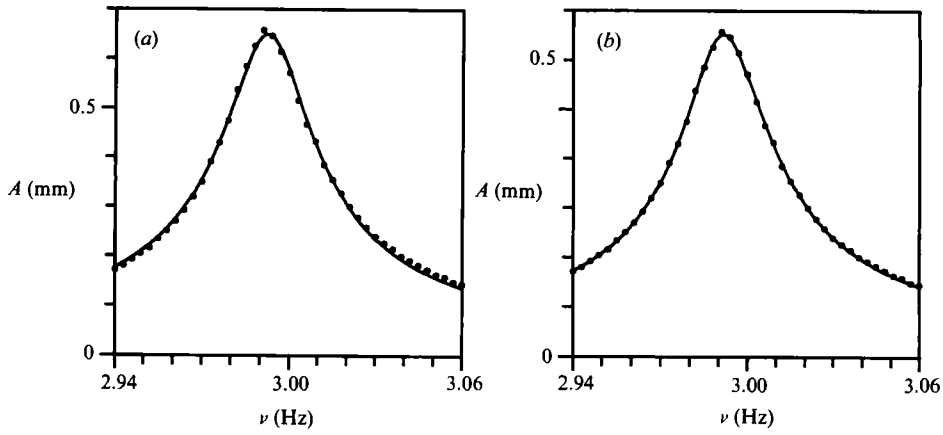

FIGURE 5. (*a*) Amplitude A versus the frequency for the fundamental mode. The parameters of the experiment are $h = 78$ mm, $a = 50.25$ mm. The product of the carriage oscillation amplitude x_0 and the square of the frequency ν^2 is held constant during the frequency sweep at the value $x_0\nu^2 = 0.0367$ mm/s^2. The solid line corresponds to the best fit of the experimental points to (3.3). The fit parameters $\bar{A}$, ν_1 and γ are: $\bar{A} = 0.00503$ mm/s^4, $\nu_1 = 2.993$ Hz, $\gamma = 29.4$ mHz. (*b*) The same experimental data as (*a*) but the solid lines correspond to the resonance curve which we obtain by using (3.3) with the experimental values of ν_1 and γ given in figures 4(*a*) and 4(*b*) and by putting $\bar{A} = 0.00503$ mm/s^4.

whilst, for $v > v_c$, one expects that the capillary contribution γ_1 decreases and goes to zero as the amplitude A increases according to (1.10) ($\gamma_l' \propto 1/A$) and thus, the limit value of γ is expected to be $\gamma = (\gamma_w)_1 + (\gamma_b)_1 + (\gamma_s)_1$.

The two viscous contributions $(\gamma_w)_1$ and $(\gamma_b)_1$ at room temperature can be calculated by using (1.3) and (1.4) with $n = 1$ and $\nu = 0.00772$ cm^2 s^{-1} (Weast 1970). We find $(\gamma_w)_1 + (\gamma_b)_1 = 16.3$ mHz. By comparing this damping coefficient with the experimental one at larger oscillation amplitudes we find $\gamma_{exp} - \gamma_{th} \approx 10$ mHz which could be interpreted by assuming that a thin viscoelastic film is present on the free surface ($(\gamma_s)_1 \approx 10$ mHz). However, it is important to notice that the surface tension of octane is very small (≈ 20 dynes/cm) and thus, one could expect that no contamination film is present on the free surface. Therefore a direct investigation to provide evidence for the presence of this surface film is needed. The difference between low- and high-amplitude values of γ could be then interpreted as due to the γ_1' capillary contribution ($\gamma_1' \approx 8$ mHz). Furthermore it is not clear how the Miles model can be extended to the case of a wetting boundary condition. In particular a moving contact line in the case of wetting boundary conditions could not be present and the effect of the draining film at the vertical walls could be dominant. Therefore the agreement between the nonlinear damping behaviour and the Miles model could be only fortuitous. A detailed theoretical analysis of the dynamic properties of the draining film would be needed in order to understand the nonlinear behaviour properly. Furthermore none of our attempts to obtain evidence for a variation of the contact angle during the motion, by direct visual analysis of the meniscus, were successful.

3.3. *Resonance frequencies and damping rate of higher-order surface modes*

In this section we investigate the resonance curves for the higher-order surface modes ($n > 1$) in (1.5)). The experimental method consisted in measuring simultaneously with a lock-in the in-phase component and the 90° out-of-phase component of the output signal of the photodetector. The laser beam (see figure 1) impinged at the

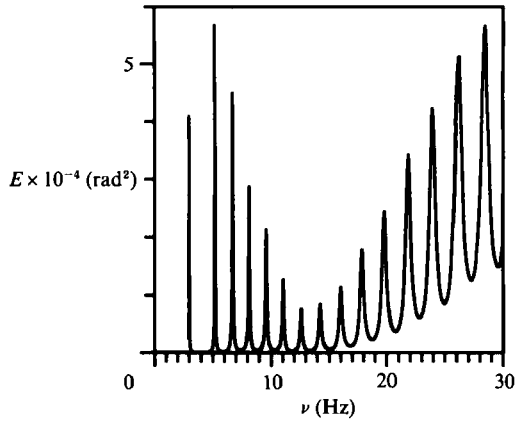

FIGURE 6. Oscillation energy $E \equiv \bar{\theta}_0^2$ of the tilt angle $\bar{\theta}_0$ at the centre of the fluid surface versus the frequency for a fixed value of x_0 (0.00408 mm). The resonances correspond to the first 15 surface modes (see (2.1)–(2.2*c*)). The depth of the fluid is $h = 78$ mm and the radius of the cylindrical container is $a = 50.25$ mm.

centre of the free surface of the fluid in such a way that the tilt angle of the free surface $\bar{\theta} \approx \tan\bar{\theta} = \partial\eta/\partial r|_{r=0,\theta=0}$ at the centre of the container could be obtained. If the carriage oscillation is $x(t) = x_0 \cos\omega t$, the tilt angle changes with time as

$$\bar{\theta}(t) = \bar{\theta}_r \cos\omega t + \bar{\theta}_i \sin\omega t \tag{3.4}$$

where $\bar{\theta}_r$ and $\bar{\theta}_i$ are the in-phase and the 90° out-of-phase amplitudes with respect to the carriage oscillation. The oscillation amplitude $\bar{\theta}_0$ is, then, defined by

$$\bar{\theta}_0 = (\bar{\theta}_r^2 + \bar{\theta}_i^2)^{\frac{1}{2}} \tag{3.5a}$$

and the adimensional energy is defined by

$$E = \bar{\theta}_0^2. \tag{3.5b}$$

The oscillation amplitude x_0 of the carriage is maintained constant during the frequency sweep. Figure 6 shows the experimental energy resonance curve for the first 15 modes where the energy E of the oscillation at a given frequency is plotted (see (3.5*b*)). We notice that the half-width of the resonances increases as the frequency increases and, thus, some overlap of resonances, for $\nu > 10$ Hz, occurs. The resonance frequencies ν_n and the damping rates γ_n of the modes can be obtained by making a fit of each resonance curve by using a Lorenzian form such as that of (3.3) with ν_n, γ_n, $\bar{A}_n$ in place of ν_1, γ_1 and $\bar{A}$, respectively. The free parameters of each fit are ν_n, γ_n and $\bar{A}_n$. We note that the phenomenological equation of motion (2.3) in the case of free-end edge boundary conditions predicts the amplitude of each mode for a given value of the amplitude of the generalized force if γ_n is known. The values of the resonance frequencies ν_n versus the product $k_n a$ are shown in figure 7(*a*). The solid line in figure 7(*a*) corresponds to the best fit of the experimental results using the theoretical expression (1.5) with the surface tension T as a free parameter. The value of T which is obtained from the best fit is $T = 20.58$ dynes/cm. Discrepancies between theory and experiment cannot be distinguished in figure 7(*a*). Therefore the difference between experimental and theoretical values of ν_n is shown in figure 7(*b*). We notice that the relative difference between the theoretical value of the resonance frequency and the experimental one is always lower than 0.5%. Therefore one can conclude that, as far as the eigenfrequencies are concerned, the free-end edge boundary conditions describe satisfactorily the behaviour of a wetting fluid.

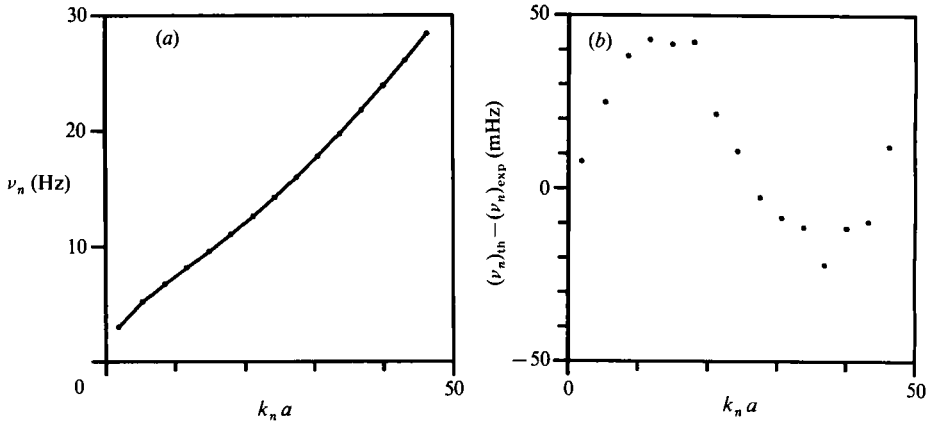

FIGURE 7. (*a*) Resonance frequency of each mode versus the product $k_n a$ between the wave vector and the container radius. The solid line corresponds to the best fit of the experimental results obtained using the theoretical expression (1.5) with the surface tension T as a free parameter and using the theoretical expression for $(\gamma_w)_n$ given in (1.4). The mass density and the kinematic viscosity coefficients are respectively, $\rho = 0.702$ g/cm^3 and $\nu = 0.00772$ cm^2 s^{-1} (Weast 1970) whilst the value of the gravity acceleration is $g = 980.5$ cm/s. The value of T given by the best fit is $T = 20.58$ dynes/cm. (*b*) Difference between the theoretical resonance frequency of the nth mode, given by (1.5), and its experimental value. The depth of the fluid is $h = 78$ mm and the radius of the cylindrical container is $a = 50.25$ mm.

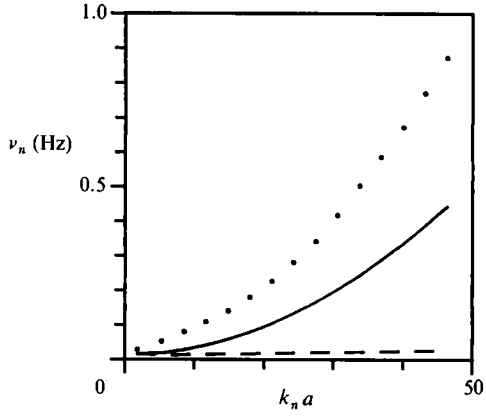

FIGURE 8. Damping rate γ_n of the nth mode versus the product $k_n a$. The broken line corresponds to the viscous damping coefficient $(\gamma_w)_n$ of (1.4). The solid line corresponds to the viscous damping $\gamma_n = (\gamma_w)_n + (\gamma_b)_n$ (see (1.3) and (1.4)). The depth of the fluid is $h = 78$ mm and the radius of the cylindrical container is $a = 50.25$ mm.

Figure 8 shows the experimental values of the damping rate γ_n versus $k_n a$. The broken line in figure 8 corresponds to the decay rate $(\gamma_w)_n$ of (1.4) as predicted by the viscous dissipation rate near a vertical wall at the first order in ϵ. The solid line corresponds to the viscous decay rate given by the sum of bulk contribution $(\gamma_b)_n$ and the wall contribution $(\gamma_w)_n$. It is evident that, although the bulk contribution is proportional to ϵ^2, it is negligible only for the first modes and becomes dominant at higher n.

A large systematic difference between theory and experiment is found for all modes. This difference could be related to the second order contributions in ϵ^2 which have been neglected in calculations of the viscous dissipation rate $(\gamma_w)_n$. Furthermore

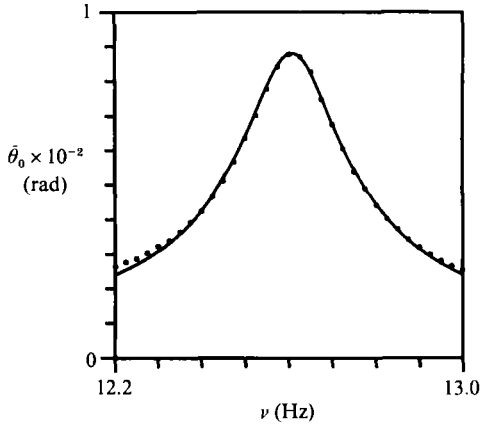

FIGURE 9. Oscillation amplitude $\bar{\theta}_0$ of the tilt angle of the free surface at the centre of the cylinder versus the frequency for the 7th mode. Points correspond to the experimental results, whilst the solid line corresponds to the best fit of the experimental data to the theoretical expression (3.6). The free parameters of the best fit are the amplitude $\bar{B}_7$, the resonance frequency ν_7 and the damping rate $\gamma_7(\bar{B}_7 = 1.57 \times 10^{-4}$, $\nu_7 = 12.609$ Hz, $\gamma_7 = 0.227$ Hz). The oscillation amplitude of the carriage is $x_0 = 0.00408$ mm, the fluid depth is $h = 78$ mm, and the cylinder radius is $a = 50.25$ mm.

other contributions, such as those considered by Miles (equations (1.6) and (1.9)), can also play an important role. Furthermore the effect of the draining film at the vertical walls could also be relevant to our experiment. Unfortunately many unknown parameters enter in the theoretical Miles expression for $(\gamma_1)_n$ and $(\gamma_s)_n$ $(\xi, C_n(k_n))$ and, thus, a direct comparison with the experimental results is not possible.

3.4. *Amplitude and phase of the forced oscillation of the free surface*

The presence of the meniscus at the vertical walls produces very important effects on the amplitude and the phase of the response of the fluid free surface to the carriage oscillation ($x(t) = x_0 \cos \omega t$). Figure 9 shows the amplitude $\overline{\theta_0}$ (see (3.5*a*)) of the mode $n = 7$ versus the frequency. Points correspond to the experimental results, whilst the solid line represents the best fit of the experimental results to the theoretical dependence of (3.6) which is obtained by solving (2.3) for a constant value of the oscillation amplitude x_0:

$$\overline{(\theta_0)_n} = \frac{\bar{B}_n \nu^2}{[(\nu_n^2 - \nu^2)^2 + \gamma_n^2 \nu^2]^{\frac{1}{2}}}. \tag{3.6}$$

$\bar{B}_n$ is a constant coefficient. We see that the phenomenological equation (3.6) describes satisfactorily the behaviour of the system. Figure 10 shows the ratio between the experimental value $\bar{B}_n$ and its theoretical value $(\bar{B}_n)_{\text{th}}$ versus the product $k_n a$. The theoretical value of $\bar{B}_n$ is calculated by solving (2.3) and by using (2.1) and (2.2). We find:

$$\overline{(B_n)_{\text{th}}} = \frac{x_0 x_n k_n^2 \tanh(k_n h)}{2N_n}, \tag{3.7}$$

where k_n is given by (2.2*b*), $N_n = N_{1,n}$ is given by (2.2*c*) and x_n is given by (2.5) (for $n = 7$ we have $k_7 = 21.16437/a$, $x_7 = 0.00316a$ and $N_7 = 0.1225$). We see clearly that the amplitudes of the modes are in satisfactory agreement with the theoretical ones only for the first modes. This clearly indicates that (2.3) does not describe the real behaviour of the surface waves.

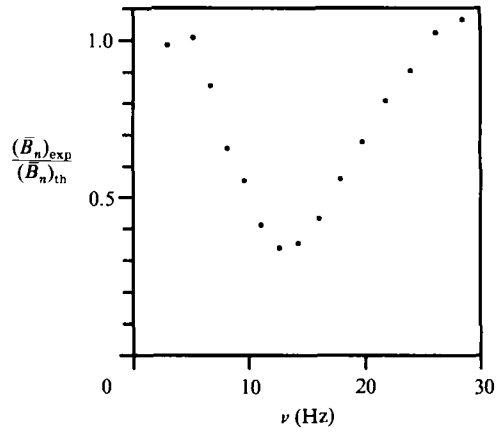

FIGURE 10. Ratio between the experimental value of $\bar{B}_n$ and the theoretical expression $(\bar{B}_n)_{th}$ of (3.7) as a function of $k_n a$. The experimental conditions are the same as figure 9.

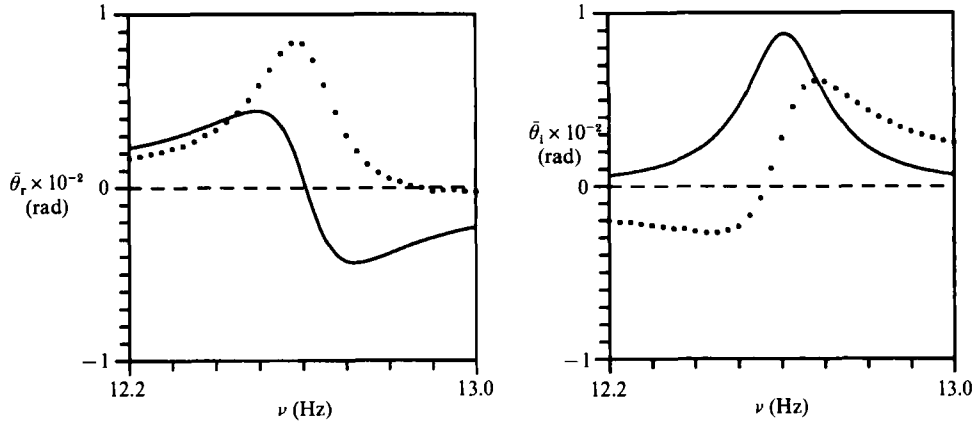

FIGURE 11. Wavevector dependence of (*a*) the in-phase oscillation amplitude $\overline{\theta_r}$ and (*b*) the 90° out-of-phase component $\overline{\theta_i}$ of the oscillation amplitude. The experimental conditions are the same as figure 9. Points correspond to the experimental results, whilst the solid line corresponds to the theoretical prediction that can be obtained by solving (2.3) for (*a*) the in-phase and (*b*) the 90° out-of-phase components of the surface oscillation and by using the parameters $\bar{B}_7$, ν_7 and γ_7 given by the best fit in figure 9 ($\bar{B}_7 = 1.57\ 10^{-4}$, $\nu_7 = 12.609$ Hz, $\gamma_7 = 0.227$ Hz).

Another stronger deviation from the predictions of (2.3) is found if one looks at the phase of the forced free oscillations. Figures 11 (*a*) and 11 (*b*) show the wavevector dependence of the in-phase and 90° out-of-phase components of the surface oscillation ($\overline{\theta_r}$ and $\overline{\theta_i}$ in (3.4)). Points correspond to the experimental results, whilst the solid lines correspond to the predictions of (2.3) using the values $\bar{B}_n$, γ_n and ν_n obtained from the fit of the amplitude spectrum as shown in figure 9. We clearly note that the two curves (experimental and theoretical) are very different, indicating the presence of a dephasing of the experimental signal with respect to that predicted by (2.3). In fact, by introducing a suitable dephasing $\Delta\phi$ to the experimental data for $\overline{\theta_r}$ and $\overline{\theta_i}$ we obtain a very good agreement with the theoretical behaviour. We define the dephased experimental amplitudes $(\overline{\theta_r})^*$ and $(\overline{\theta_i})^*$ as

$$(\overline{\theta_r})^* = (\overline{\theta_r})_{exp} \cos(-\Delta\phi) + (\overline{\theta_i})_{exp} \sin(-\Delta\phi) \tag{3.8}$$

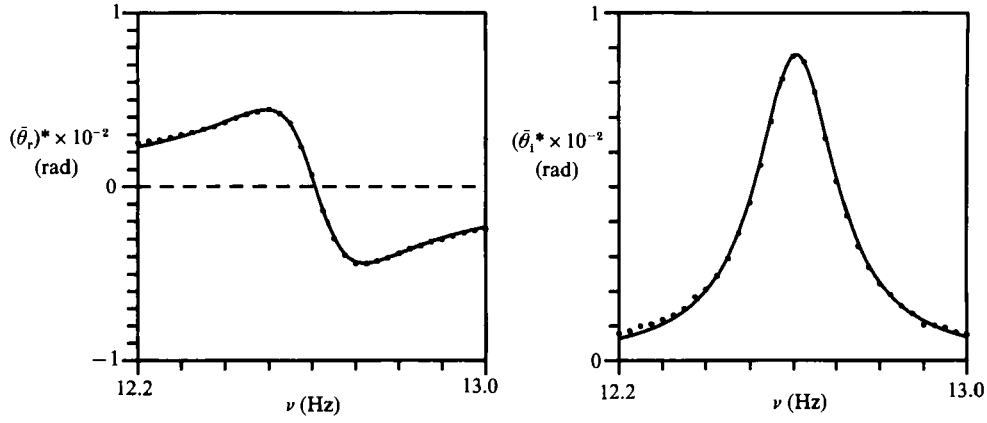

FIGURE 12. (*a*) Dephased experimental results for the resonance $n = 7$. Points correspond to the dephased experimental data $(\overline{\theta_r})^*$ as defined in (3.8) whilst the solid line corresponds to the theoretical expression obtained by solving (2.3) for the in-phase component. $\Delta\phi =$ is given by the best fit of $(\overline{\theta_r})^*$ with respect to the theoretical form. The best fit gives $\Delta\phi = 67° 43'$. (*b*) As (*a*) but for the 90° out-of-phase component $(\overline{\theta_i})^*$, for which the best fit gives $\Delta\phi = 67° 5'$.

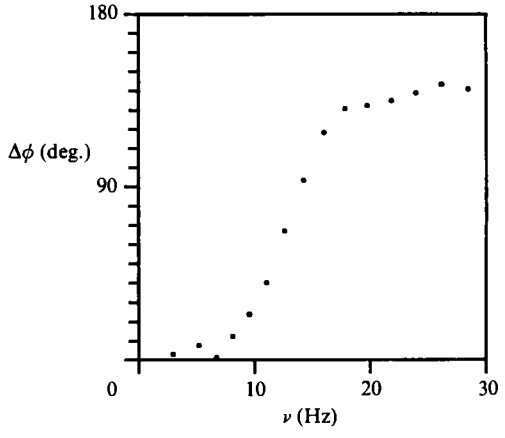

FIGURE 13. Dephasing $\Delta\phi$ which must be introduced in the experimental data to fit the experimental resonances curves for the $\overline{\theta_r}$ and $\overline{\theta_i}$ (see figures 12*a* and 12*b*).

and
$$(\overline{\theta_i})^* = (\overline{\theta_r})_{exp} \sin(-\Delta\phi) + (\overline{\theta_i})_{exp} \cos(-\Delta\phi). \tag{3.9}$$

The best fit of these new dephased experimental data with respect to the theoretical curves of figures 11 (*a*) and 11 (*b*) by using $\Delta\phi$ as a free parameter is shown in figures 12 (*a*) and 12 (*b*) respectively. We find a satisfactory agreement between the dephased data and theoretical curves by obtaining best fit values of $\Delta\phi$ for the two curves which coincide, within the experimental accuracy ($\Delta\phi = 67° 43'$ for $(\overline{\theta_r})^*$ and $\Delta\phi = 67° 5'$ for $(\overline{\theta_i})^*$. By using the same procedure to fit all the resonances ($n = 1, \ldots, 15$ in figure 6) one obtains the dependence of this dephasing $\Delta\phi_n$ as a function of the number of the mode as shown in figure 13. The dephasing is negligible for the first excited mode and greatly increases as n increases to reach an almost constant value $\approx 150°$ for large n.

An analogous dephasing is found by using water wetting a cylindrical basin. *This effect must be strictly related to the boundary conditions at the vertical walls* (*contact angle* $\theta = 0$). In fact, repeating the same experiment using water in a Plexiglas cylindrical

container where the static contact angle is $\theta = 66°$, we do not find any appreciable dephasing and the phase behaviour agrees satisfactorily with the simple behaviour predicted by (2.3).

This effect, together with the depression of the oscillation amplitude shown in figure 10, is probably related to the interaction between the oscillation of the free surface and the induced oscillation of the meniscus. In fact we note that the minimum of the surface wave amplitude in figure 10 occurs when the wavevector of the gravity–capillary surface wave is just of the order of the inverse of the capillary length $\lambda = (T/\rho g)^{\frac{1}{2}}$.

4. Conclusions

In this paper the behaviour of resonant surface capillary–gravity waves in a cylindrical basin subjected to a horizontal oscillation has been investigated. In the case of wetting boundary conditions on the vertical walls the frequency of modes is in good agreement with that predicted by assuming the standard boundary conditions (free-end edge). Therefore measuring the frequency of modes versus the wavevector furnishes a simple and accurate method of obtaining the surface tension of the fluid.

The free decay of surface oscillations and the amplitude and phase of the response of the fluid surface to a horizontal periodic oscillation have a more complex behaviour. In particular the free decay exhibits a non-exponential time-dependence of the dissipation coefficient γ which indicates a dependence of γ on the amplitude of the surface wave. A similar nonlinear dependence of γ on the amplitude has been predicted by Miles (1967) as due to the capillary effects at the vertical walls. An analogous but very weak dependence on the amplitude has been also observed for the frequency of the mode ($(\Delta\nu)_{\max}/\nu \approx 0.2\%$). This dependence greatly depends on the kind of boundary conditions at the walls and, thus, it seems to be related to the fluid meniscus.

Finally a strong dephasing (up to 150°) between the experimental forced oscillations of the free surface and those predicted by a simple phenomenological model was observed. This effect is strictly connected with the presence of a wetting boundary condition for the fluid at the vertical walls.

We acknowledge Professor C. Festa for his helpful comments and advices.

REFERENCES

Ablett, R. 1923 An investigation of the angle of contact between paraffin wax and water. *Phil. Mag.* **46**, 244–256.

Benjamin, T. B. & Scott, J. C. 1979 Gravity–capillary waves with edge constraints. *J. Fluid Mech.* **92**, 241–267.

Case, K. M. & Parkinson, W. C. 1957 Damping of surface waves in an incompressible fluid. *J. Fluid Mech.* **2**, 172–184.

Douady, S. 1988 Capillary–gravity surface wave modes in a closed vessel with edge constraint: eigen-frequency and dissipation. *Woods Hole Ocean Inst. Tech. Rep.*, WHOI-88.

Douady, S. 1990 Experimental study of the Faraday instability. *J. Fluid Mech.* **221**, 383–409.

Dussan V., E. B. 1979 On the spreading of liquids on solid surfaces: static and dynamic contact lines. *Ann. Rev. Fluid Mech.* **11**, 371–400.

Funakoshi, M. & Inoue, S. 1988 Surface waves due to resonant horizontal oscillation. *J. Fluid Mech.* **192**, 219–247.

GRAHAM-EAGLE, J. 1983 A new method for calculating eigenvalues with application to gravity–capillary waves with edge constraints. *Math. Proc. Camb. Phil. Soc.* **94**, 553–564.

GRAHAM-EAGLE, J. 1984 Gravity–capillary waves with edge constraints. D.Phil. thesis, University of Oxford.

HOCKING, L. M. 1987*a* The damping of capillary–gravity waves at a rigid boundary. *J. Fluid Mech.* **179**, 253–266.

HOCKING, L. M. 1987*b* Waves produced by a vertically oscillating plate. *J. Fluid Mech.* **179**, 267–281.

KEULEGAN, G. H. 1959 Energy dissipation in standing waves in rectangular basins. *J. Fluid Mech.* **6**, 33.

LAMB, H. 1932 *Hydrodynamics*, 6th edn. Cambridge University Press.

MEI, C. C. & LIU, L. F. 1973 The damping of surface gravity wave in a bounded liquid. *J. Fluid Mech.* **59**, 239–256.

MILES, J. W. 1967 Surface-wave damping in closed basins. *Proc. R. Soc. Lond.* A **297**, 459–475.

MILES, J. W. 1976 Nonlinear surface waves in closed basins. *J. Fluid Mech.* **75**, 419–448.

MILES, J. W. 1984 Resonantly forced gravity waves in a circular cylinder. *J. Fluid Mech.* **149**, 15–45.

NOBILI, M., CILIBERTO, S., COCCIARO, B., FAETTI, S. & FRONZONI, L. 1988 Time-dependent surface waves in a horizontally oscillating container. *Europhys. Lett.* **7**, 587–592.

URSELL, F. 1952 Edge waves on a sloping beach. *Proc. R. Soc. Lond.* A **214**, 79–97.

VAN DORN, W. G. 1966 Boundary dissipation of oscillatory waves. *J. Fluid Mech.* **24**, 769–779.

WEAST, R. C. 197 *Handbook of Chemistry and Physics*. The Chemical Rubber Co. 18901 Cranwood Parkway, Cleveland, Ohio, 44128.